Effects of Mass Ratio Heterogeneity and Coating-Related Optical Characteristics on the Light Absorption Enhancement of Black Carbon-Containing Particles

Jing Wei[1], Jin-Mei Ding[2], Yao Song[1], Xiao-Yuan Wang[2], Xiang-Yu Pei[1], Sheng-Chen Xu[2], Fei Zhang[1], Zheng-Ning Xu[1], Xu-Dong Tian[2], Bing-Ye Xu[2], Zhi-Bin Wang[1,3]

[1] State Key Laboratory of Soil Pollution Control and Safety, Zhejiang Provincial Key Laboratory of Organic Pollution Process and Control, College of Environmental and Resource Sciences, Zhejiang University, Hangzhou 310058, China

[2] Ecological and Environmental Monitoring Center of Zhejiang Province, Hangzhou 310012, China

[3] ZJU-Hangzhou Global Scientific and Technological Innovation Center, Zhejiang University, Hangzhou 311200, China

Correspondence: Bing-Ye Xu (xubingye@zjemc.org.cn) and Zhi-Bin Wang (wangzhibin@zju.edu.cn)

Abstract

Black carbon (BC) is a strong climate forcer, but considerable uncertainty remains in estimating its radiative impact, largely due to persistent gaps between observed and modeled light absorption enhancement (E_{abs}). In this study, we employed a Centrifugal Particle Mass Analyzer and Single Particle Soot Photometer tandem system to characterize mass ratio (M_R, coating-to-BC) of BC-containing particles in Hangzhou, China. Observations across a field campaign revealed low, medium, and high E_{abs} values under varying atmospheric conditions. The uniform core-shell Mie model overestimated E_{abs}, particularly during clean periods (low E_{abs}). To address this, we developed an observationally constrained parameterization for transition-state particles based on M_R-dependent optical transitions behaviors. This approach effectively reconciles modeled and measured E_{abs} across varying pollution conditions. It also emphasizes the importance of incorporating M_R heterogeneity and transition-state optical behavior to improve BC light absorption estimates and reduce uncertainties in assessing radiative effects.

1 Introduce

Black carbon (BC) is a strongly light-absorbing aerosol that effectively absorbs solar radiation, warms the atmosphere, and contributes to direct radiative forcing (DRF) (Bond and Bergstrom, 2006; Seinfeld, 2008). According to IPCC assessments, the global effective DRF of BC ranges from −0.28 to 0.41 W/m^2 (Szopa et al., 2021). To represent the effect of BC particle coatings on absorption, most climate models (Bauer et al., 2013; Chen et al., 2024; Stier et al., 2005; Wang et al., 2023; Zhang et al., 2025b) estimate BC light absorption enhancement (E_{abs}) using Mie theory, defined as the ratio of absorption by coated BC to that of uncoated BC cores, under the assumption of a uniform core-shell structure where BC core is fully encapsulated by coating materials. This approach predicts a monotonic increase in E_{abs} with the coating-to-core mass ratio (M_R), often reaching values up to ~2, consistent with laboratory results (Peng et al., 2016) and the pyroCb smoke (Beeler et al., 2024). However, field observations commonly report lower E_{abs} values, typically around 1.4 and sometimes as low as 1.09 (Cappa et al., 2012; Huang et al., 2024), although some studies have found moderate E_{abs} values, with maxima reaching approximately 1.5 (Liu et al., 2015b). This discrepancy mainly stems from the oversimplified assumptions in Mie theory, which fail to capture the real atmospheric complexity in BC size distribution, coating configuration, and mixing state (Wang et al., 2021c). Previous microscopy-based single-particle studied (e.g., TEM and SEM) have visually demonstrated that the ambient BC particles exhibit diverse coating structures and highly heterogeneous mixing states, providing direct evidence of deviation from the idealized core-shell assumption (Adachi et al., 2010; Adachi and Buseck, 2013; China et al., 2013; Wang et al., 2021c). Although microscopy techniques are not employed in this work, these findings highlight the importance of realistically representing BC mixing state and coating characteristics when modeling optical properties. The mismatch between model assumptions and observations has motivated efforts to refine the conceptual modeling approaches for BC aging and coating evolution, which forms the focus of this study.

60　　　　A number of studies have explored the discrepancies in BC E_{abs} from various
61　perspectives. Particle-resolved modeling has demonstrated that both particle-to-particle
62　heterogeneity in M_R and deviations from the idealized core-shell structure can strongly
63　influence absorption estimates (Fierce et al., 2020). In particular, non-uniform or partial
64　coatings at low M_R can lead to the overestimation of E_{abs} by traditional core-shell
65　models. However, these factors alone tend to cannot explain the low E_{abs} frequently
66　observed under high M_R conditions (Huang et al., 2024). Atmospheric BC particles also
67　exhibit substantial variability in their internal mixing state during aging. Fresh BC
68　exhibit a branched structure that collapses into compact shapes with reduced light
69　absorption cross-sections during aging (Moteki and Kondo, 2007; Romshoo et al., 2024;
70　Li et al., 2024; Radney et al., 2014; Corbin et al., 2023). Early aging stage feature
71　uneven coatings, while aged particles show BC core either encapsulated or located near
72　the particle surface (Zhang et al., 2008; Adachi and Buseck, 2013). These aging features
73　are consistent with single-particle observations showing the progressive collapse and
74　coating thickening of BC aggregates during atmospheric processing (Adachi et al., 2016;
75　Ueda et al., 2016), which support the conceptual framework adopted in this study.
76　Recent studies further suggest that the proportion of non-spherical BC particles and the
77　position of the BC core may be key factors contributing to low E_{abs}, leading to an
78　overestimation by core-shell model (Huang et al., 2024; Chen et al., 2024; Zhang et al.,
79　2022). Although this study does not involve direct microscopic measurements or
80　detailed particle-resolved modeling, our work aims to refine the conceptual
81　representation of BC aging and coating evolution to better capture M_R-related optical
82　behavior under ambient conditions.

83　　　　In this study, a suite of state-of-the-art instruments were employed to
84　simultaneously capture the magnitude and temporal of BC M_R in Hangzhou, China
85　(Zhang et al., 2025a; Qian et al., 2025). The ratio of SP2-measured single-particle
86　scattering cross sections to the core-shell Mie theory simulated values was used as an
87　observational proxy to characterize M_R-dependent optical transitions of BC-containing
88　particles (Liu et al., 2017a; Liu et al., 2020). Field measurements revealed the
89　coexistence of high, medium, and low E_{abs} under high bulk-averaged M_R conditions.
90　Based on these observations, the influences of M_R heterogeneity and M_R-dependent
91　optical behavior were quantified to reconcile discrepancies in E_{abs} between model
92　predictions and field observations. Subsequently, an observationally constrained
93　parameterization for "transition-state" BC-containing particles was refined to better
94　reproduce measured E_{abs} under different ambient atmospheric conditions. This study
95　underscores the importance of simultaneously accounting for M_R heterogeneity and M_R-
96　dependent optical transitions when predicting E_{abs}, offering insights that can help reduce
97　uncertainties in estimates of BC direct radiative forcing.

98　**2 Methods**

99　**2.1 Overview of the field campaign and instrumentation**

100　The field measurements were conducted at the Central Air Quality Assurance
101　Monitoring Station (30.25°N,120.24°E) in Hangzhou from 3th Sept., 2023 to 13th Oct.,

2023. The sampling site is located just 100 meters from the Qiantang River in the western part of Hangzhou, with major traffic routes within 3 kilometers to the northeast and southwest of the station. The schematic of the instrumentation is provided in Fig. S1. Aerosols were sampled after passing through a $PM_{2.5}$ impactor and then dried through a diffusion dryer before reaching subsequent instruments.

The mass of a BC-containing particle (M_p) and of the BC core (M_{BC_core}) were simultaneously obtained by a Centrifugal Particle Mass Analyzer (CPMA, Cambustion) and a single-particle soot photometer (SP2, DMT Inc.) tandem system. The CPMA classifies particles according to their total mass and has been described in detail by Olfert and Collings (2005). According to the instrument manual, the mass accuracy of the CPMA is approximately 5%. The SP2 measures particle incandescence and scattering to determine BC core mass and optical properties (Stephens et al., 2003; Moteki and Kondo, 2010; Gysel et al., 2011; Schwarz et al., 2022), and the uncertainty associated with the SP2-derived BC core mass (M_{BC_core}) is approximately 10% (Laborde et al., 2012). Previous studies have applied the tandem CPMA-SP2 set up (Cross et al., 2010; Liu et al., 2022; Naseri et al., 2022; Zanatta et al., 2025). In this work, SP2 was calibrated using size-resolved Aquadag aerosols (DMT, 2011) (Fig. S2c and d) following the procedures described by Baumgardner et al. (2012) and Laborde et al. (2012). In this setup, particles with known mass (M_p) selected by CPMA were injected into the SP2.

The CPMA was operated over M_p setpoints ranging from 0.9 fg to 30 fg, logarithmically spaced into ten intervals (0.93 fg, 1.37 fg, 2.02 fg, 2.97 fg, 4.36 fg, 6.40 fg, 9.39 fg, 13.78 fg, 20.22 fg and 29.68 fg), then the mass of BC core was measured by SP2. The duration of one set point cycle was 1 hour, with each M_p point sampling for 5 minutes, and all M_p points was sampling for total of 50 minutes. The remaining 10 minutes were divided into 4 minutes for instrument stabilization and 6 minutes for measuring all BC-containing particles when the valve was switched to the single SP2 line. During further data analysis, particles with $M_p = 0.93$ fg and $M_p = 1.37$ fg exhibited excessively noisy scattering signals, likely due to weak signal intensity and low signal-to-noise ratio for small particles, and were therefore excluded from subsequent statistical analysis.

In the subsequent data processing, measurements from the CPMA-SP2 system were first corrected for multiple charging effects using a peak-resolved subtraction approach. An X-ray aerosol neutralizer (TSI 3088) installed upstream of the CPMA produced a known bipolar charge distribution, resulting in discrete mass modes corresponding to singly and multiply charged particles in the CPMA mass spectra. The CPMA transfer function was calculated based on the CPMA geometric and operational parameters, with a set mass resolution $R_m=8$ (Text S1), ensuring that charge-dependent mass modes were sufficiently resolved. Under these conditions, mass peaks attributable to multiply charged particles (q > 1) could be explicitly identified based on their expected mass-to-charge relationships and quantitatively subtracted, while the singly charged mode corresponding to the CPMA setpoint was retained for subsequent analysis. This peak-resolved subtraction represents a simplified, charge-resolved inversion, which differs from full matrix-based inversion schemes (Naseri et al., 2024;

Naseri et al., 2021) , but is appropriate when charge-dependent mass modes are well resolved and non-overlapping. Additional corrections, including SP2 detection efficiency, and instrumental time delay, were applied as described in Text S1. The mass of each BC core ($M_{\text{BC\_core}}$) was then calculated from the SP2 incandescence signal using the calibration described above, with a correction factor of 0.75 applied to the peak height (Liu et al., 2020; Liu et al., 2014; Zhang et al., 2018; Gysel et al., 2011). The SP2 scattering signal was calibrated with polystyrene latex spheres (PSL) of known sizes (210 nm, 270 nm and 310 nm) (Fig. S2b). Additionally, the calibration of the scattering and the incandescence channels was performed before and after the measurement campaign.

The mass concentrations of non-refractive OA, nitrate, sulfate, ammonium and chloride was measured by time-of-flight aerosol chemical speciation monitor with extended resolution (ToF-ACSM X, Aerodyne). Instrument principles, calibration procedures, and operational details for the ToF-ACSM X are described in a previous study of ours (Zhang et al., 2025a). The aerosol extinction and scattering coefficient (Fig. S3) at wavelength of 440, 530 and 630 nm were measured by Multi-Wavelength Cavity Attenuated Phase Shift Single-Scattering Albedo Monitor (CAPS-ALB, Shoreline) (Weber et al., 2022). Absorption was calculated as the difference between extinction and scattering, with estimated uncertainties of ~1-10% for both extinction and scattering (Modini et al., 2021), leading to a conservative absorption uncertainty of ~15-20% for the submicron BC particles considered. No explicit truncation correction was applied, as the analysis focuses on the relative enhancement of absorption with M_R rather than absolute values. In this study, only the measurements at 630 nm were used for subsequent analysis, as this wavelength is minimally affected by brown carbon absorption. Besides, the aerosol scattering coefficient at wavelength of 450 nm, 525 nm, and 635 nm was also measured by Multi Wavelength Integrating Nephelometer (Abbreviation: Nephelometer, Aurora 3000, Acoem) (Schloesser, 2016). The slope of the scattering coefficient measured by CAPS-ALB and Nephelometer at corresponding wavelength was close to 1 (Fig. S4), indicating the all data are reliable for further analysis. Besides, before sampling, the scattering coefficient of CAPS-ALB and Nephelometer at every wavelength was calibrated using PSL spheres. Monodisperse PSL particles of different diameters (100 nm, 150 nm, 200 nm and 300 nm) were selected using a Differential Mobility Analyzer (DMA) and introduced into the instruments, enabling accurate measurement of their scattering cross section (C_{sca}). The slope of the C_{sca} measured by CAPS-ALB (or the Nephelometer) and modeled by Mie theory was close to 1 (Fig. S5), indicating the reliability of the CAPS-ALB and Nephelometer. The lower detection limit of the Nephelometer at all three wavelengths was 0.3 Mm^{-1} with a 60-second integration time, while that of the CAPS-ALB was 1 Mm^{-1} with 30-second integration time.

2.2 Mixing state and M_R-dependent optical transitions of the particle-resolved BC-containing particles

Under the assumption of singly charged particles, the mixing state of a single BC-containing particle can be represented by the mass ratio of the BC coating to the BC

189   core, without relying on assumptions about particle morphology or coating structure,

$$M_R = (M_p - M_{BC\_core})/M_{BC\_core} \tag{1}$$

190   where M_p and M_{BC_core} were the total mass and the BC core mass of each BC-containing
191   particle, respectively. Considering the uncertainties of M_p (5%) and M_{BC_core} (10%), the
192   uncertainty of M_R for a single BC-containing particle was approximately 11% (Text S2).
193   Then M_R was converted to the bulk-averaged M_R to be compared with the measured
194   E_{abs} in bulk particles by summing of total coating and BC core mass of BC-containing
195   particles each hour,

$$bulk - averaged\ M_R = \frac{\sum_i M_{R,i} \times M_{BC\_core,i}}{\sum_i M_{BC\_core,i}} \tag{2}$$

196   where i was the ith single BC-containing particle. Propagating these uncertainties to the
197   hourly mass-weighted calculation resulted in an uncertainty of approximately 7% for
198   the bulk-averaged M_R (Text S2). The data measured by CPMA-SP2 were corrected via
199   several steps, including (1) correction of delay time, (2) multi-charged particles and (3)
200   collection efficiency (for details, see Text S1).

201   The M_R-dependent optical transitions of BC-containing particles were further
202   derived from SP2 measurements at a wavelength of 1064 nm. In the CPMA-SP2 system,
203   when both M_p and M_{BC_core} are known, the modeled scattering cross section ($C_{sca\_modeled}$)
204   of BC-containing particles can be derived using Mie theory (Wang et al., 2021a). This
205   calculation assumes a core-shell structure, with the BC core having a refractive index
206   of 2.26-1.26i (Liu et al., 2017a; Zhao et al., 2020) and the non-absorbing coating
207   characterized by a refractive index of 1.48 and a density of 1.5 g cm^{-3} at a wavelength
208   of 1064 nm (Liu et al., 2015a). The measured scattering cross section ($C_{sca\_measured}$) was
209   obtained from the SP2 using the leading-edge-only (LEO) technique, which
210   reconstructs the scattering signal as BC-containing particles pass through the SP2 laser
211   beam due to partial evaporation of refractory-absorbing material. The validity of this
212   reconstruction relies on the assumption that the leading-edge data used for fitting
213   represents an unperturbed particle, as extensively reported in previous studies (Liu et
214   al., 2014; Zhang et al., 2016; Brooks et al., 2019; Gao et al., 2007; Zhang et al., 2020).
215   Note only particles with successfully fitted LEO signals are considered in the optical
216   property calculations. By comparing $C_{sca\_measured}$ with $C_{sca\_modeled}$, the M_R-dependent
217   optical behavior of BC-containing particles can be inferred, particularly for transition-
218   state particles. This comparison captures how variations in coating-to-core mass ratio
219   influence scattering, providing observational constraints on the optical evolution of BC
220   during aging (Liu et al., 2017a; Liu et al., 2020). Further methodological details are
221   provided in Section 3.

222   2.3 The measured and modeled E_{abs}

223   The light absorption enhancement of BC-containing particles is defined as the ratio
224   of the mass absorption cross section (MAC) of the coated and uncoated BC-containing
225   particles (Eq. 3), Here, MAC is defined as the particle light absorption cross section
226   normalized by the BC mass, representing the light absorption per unit mass of BC.

$$E_{abs\_measured} = \frac{MAC_{BC\_coated\_measured}}{MAC_{BC\_core\_measured}} \qquad (3)$$

227 where $E_{abs\_measured}$ is the measured light absorption enhancement, and
228 $MAC_{BC\_core\_measured}$ is the mass absorption cross section for uncoated BC particles. The
229 value of $MAC_{BC\_core\_measured}$ was obtained by extrapolating $MAC_{BC\_coated\_measured}$ to the
230 limit of bulk-averaged $M_R = 0$ using linear regression. The $MAC_{BC\_core\_measured}$ at
231 wavelength of 630 nm was 9.08 ± 0.53 m^2 g^{-1} (mean $\pm$ 90% confidence Interval) (Fig.
232 S6). Based on our error propagation analysis, which accounts for measurement
233 uncertainties in particle absorption and BC mass as well as the standard error of the
234 extrapolation, the estimated uncertainty of $MAC_{BC\_core\_measured}$ is approximately 19-23%
235 (Text S2). And the uncertainty of $E_{abs\_measured}$ is approximately 26 - 32% (Text S2). Note
236 the $MAC_{BC\_core\_measured}$ is slightly higher than the value of 7.5 m^2 g^{-1} recommended by
237 Bond and Bergstrom (2006) but still within the range reported by other study (~6.5 - 17
238 m^2 g^{-1}) (Zanatta et al., 2016), likely due to variations in measurement methods, and site-
239 specific atmospheric conditions. Importantly, at high bulk-averaged M_R (≈ 5), the
240 measured MAC did not approach the laboratory-based absorption enhancement (E_{abs}
241 ≈ 2) reported for idealized core-shell soot particles (Cappa et al., 2012). The observed
242 limited E_{abs} ≈ 1.1~1.5 is consistent with ambient studies and can be explained by the
243 complexity of ambient particles: the heterogeneity of particle-resolved M_R and
244 morphology can reduce absorption enhancement by ~20-70% relative to idealized
245 internal mixtures (Huang et al., 2024; Cappa et al., 2019), while variations in coating
246 composition and instrumental uncertainties contribute additional variability but are
247 considered secondary factors. These high-time-resolution field measurements therefore
248 provide quantitative constraints on BC E_{abs} under realistic atmospheric conditions,
249 complementing laboratory studies and informing model evaluations of aerosol optical
250 properties and regional radiative effects.
251   The commonly used models for calculating the optical properties of BC-
252 containing particles include Core-shell Mie theory (Cappa et al., 2012), T-matrix (Wu
253 et al., 2020), and discrete dipole approximation (DDA) (Kahnert and Kanngießer, 2020)
254 and the generalized Mie Model (Kahnert and Kanngießer, 2020). Among them, T-
255 matrix, and DDA fully account for detailed particle structure by incorporating three-
256 dimensional parameters such as particle configuration and internal mixing state (Wu et
257 al., 2020). In contrast, Core-shell Mie theory relies solely on the BC core size (D_c) and
258 coating thickness (D_p/D_c). Given the measurement data available in this study, the Core-
259 shell Mie theory was used to calculate the E_{abs} of BC-containing particles at a
260 wavelength of 630 nm. The refractive index (RI) of BC and its coatings are assumed to
261 be n=1.85+0.71i and n=1.5+0i at a wavelength of 630 nm (Liu et al., 2015a; Liu et al.,
262 2014). The size of BC core and coating thickness was directly measured by CPMA-SP2
263 tandem system. For the uniform core-shell assumption, the M_R of every D_c was equal
264 to bulk-averaged M_R (Section 2.2), as described by Cappa et al. (2019) and Liu et al.
265 (2017a). Then the particle-resolved Core-shell Mie theory was employed to calculate
266 the MAC_{BC} of individual BC-containing particles. After obtaining the particle-resolved
267 MAC, we can calculate the MAC of BC particle ensembles as

$$MAC_{BC\_coated\_modeled} = \frac{\sum_i MAC_{BC\_coated\_modeled,i} \times M_{BC\_core,i}}{\sum_i M_{BC\_core,i}} \tag{4}$$

where i denotes the ith BC-containing particle, and $MAC_{BC\_coated\_modeled,i}$ and $M_{BC\_core,i}$ represent the particle-resolved modeled MAC of coated BC and the mass of the BC core, respectively Then, the modeled E_{abs} of BC particle ensembles are calculated as the ratio of MAC_{BC_coated} to MAC_{BC_core}. Note that the MAC_{BC_core} here is calculated using the core-shell Mie model when $D_p / D_c = 1$.

To better characterize the influence of coating on the optical response of BC-containing particles, we derived a parameter based on the ratio between the SP2-measured scattering cross section ($C_{sca\_measured}$) and the values calculated using the core–shell Mie model ($C_{sca\_modeled}$) at 1064 nm. This ratio changes consistently with M_R, providing an optical indicator of coating-induced variations in particle properties. An empirical $C_{sca\_measured}$-M_R relationship (Fig. 3d-f) was then developed using SP2 observations, and subsequently applied to infer the MAC of transition-state BC-containing particles. The bulk-averaged MAC was obtained by integrating the inferred MAC over the entire BC population.

3 Results and discussions

3.1 Direct observation of different E_{abs}.

The average $E_{abs\_measured}$ during the sampling period in Hangzhou is 1.28 ± 0.02 (mean $\pm$ 90% confidence Interval, the same below) at wavelength of 630 nm, and the bulk-averaged M_R is 3.32 ± 0.06, with average $E_{abs\_measured}$ values of 1.09 ± 0.02, 1.84 ± 0.07, and 1.55 ± 0.04 for Case 1, Case 2, and Case 3, respectively. To investigate the temporal evolution of BC coating, the observation period was classified into three cases based on the variation of $E_{abs\_measured}$, using E_{abs}=1.5 as the reference threshold (Fig.1). Case 1 (September 3-23 and October 1-7, 2023) corresponds to $E_{abs\_measured}$ significantly below 1.5. These periods were characterized by relatively low non-refractory PM$_1$ concentrations and high wind speeds (WS = 0.94 ± 0.04 m/s). Back-trajectory analysis further shows that Case 1 was dominated by clean marine and nearby local air masses, resulting in relatively clean and weakly aged conditions (Fig. 1a). Case 2 (September 24–30) corresponds to periods when $E_{abs\_measured}$ remained continuously higher than 1.5. This episode occurred under stagnant meteorological conditions-characterized by weak winds (WS = 0.81 ± 0.02 m/s) and elevated relative humidity (RH = $81.34 \pm 17.12\%$) - that favored secondary aerosol formation. Back-trajectory analysis further indicates that Case 2 was dominated by air masses transported from Jiangsu and passing through northern Zhejiang, enhancing pollutant accumulation and promoting more aged BC conditions. Case 3 includes periods when $E_{abs\_measured}$ persistently fluctuated around 1.5. The air masses during this period were a mixture of polluted inland outflow and clean marine inflow, suggesting the air masses were moderately aged–which explains the intermediate E_{abs}.

Some studies conducted in cities such as Beijing (Peng et al., 2016), Shanghai (Zhai et al., 2022) have observed a notable increase in $E_{abs\_measured}$. In contrast, in cleaner regions like Shenzhen (Huang et al., 2024), Houston (Peng et al., 2016) and California

(Cappa et al., 2012; Cappa et al., 2019), even when R_{BC} reached approximately 5, $E_{abs\_measured}$ often showed minimal enhancement. Our observations captured a wide range of $E_{abs\_measured}$ values (0.92~1.84), encompassing high, medium, and low levels. In these three cases, $E_{abs\_measured}$ exhibited distinct evolution patterns during the aging of BC-containing particles (Fig. 1), with its dependence on bulk-averaged M_R being minimal in Case 1, moderate in Case 3, and strongest in Case 2. The differences among the three cases may also be associated with variations in meteorological conditions, air mass origin, and chemical composition. On the other hand, in Case 2, the E_{abs} calculated using the traditional core-shell Mie model ($E_{abs\_uniform}$) reasonably agrees with the $E_{abs\_measured}$, whereas Case 3 shows a slightly lower level of consistency. However, in Case 1, the $E_{abs\_uniform}$ predicted by the traditional core-shell Mie model is significantly higher than the $E_{abs\_measured}$. In our subsequent analysis, we will address this discrepancy by exploring both heterogeneity of M_R and M_R-dependent transitions in optical properties.
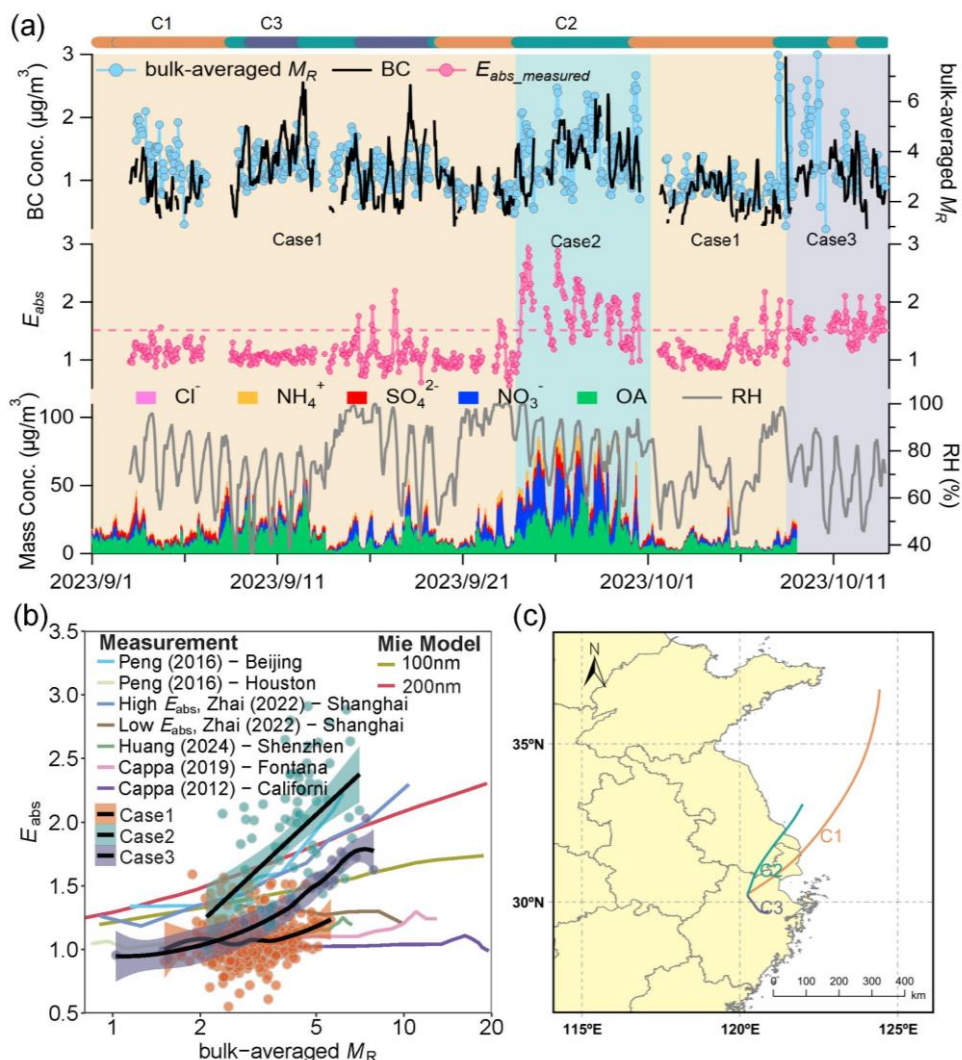
Figure. 1 (a) The time series of BC concentrations, bulk-averaged M_R, measured E_{abs}, and the chemical components (including organics, nitrate, sulfate, ammonium and chloride) measured by TOF-ACSM X, as well as relatively humidity (RH). Shaded regions indicate different cases: light yellow for Case 1, blue-green for Case 2, and gray

for Case 3. (b) Comparison of measured E_{abs} in different observation periods and with previous studies (Peng et al., 2016; Cappa et al., 2012; Zhai et al., 2022; Cappa et al., 2019; Huang et al., 2024). The black solid line represents the fitted smoothing curve of bulk-averaged M_R and measured E_{abs}, with the shaded area indicating the 95% confidence interval of the fit. (c) Mean 48-h back-trajectory simulations initialized at 100 m above ground level. The back trajectories were calculated using the Hybrid Single-Particle Lagrangian Integrated Trajectory (HYSPLIT) model driven by GDAS meteorological fields.

3.2 Role of mixing state heterogeneity in E_{abs} and direct evidence of M_R-dependent optical transitions of BC-containing particles.

The coating-to-BC mass ratio (M_R) and the ratio of measured to modeled scattering cross sections were used to quantify the mixing state and associated optical transitions behavior of BC-containing particles, with M_R serving as an important indicator of BC aging (Zeng et al., 2024; Li et al., 2024; Liu et al., 2017a). Fig. 2a and 2b illustrated significant differences in the normalized number distribution of BC-containing particles at M_p = 4.35 fg and 9.38 fg during different observation periods. Specifically, during Case 2 and Case 3, the M_R presents a unimodal distribution, with the peak value increasing with increasing M_p. In contrast, during Case 1, the M_R exhibits a distinct bimodal distribution, and both peak positions shift toward higher M_R values as M_p increases. For example, when M_p = 4.35 fg, the two peaks occur at M_R = 1 fg and 4.2 fg, respectively, whereas at M_p = 9.38 fg, they shift to M_R = 1.8 fg and 8.0 fg, respectively. The standard deviation (SD) of $\log_{10}(M_R)$ was used to characterize the heterogeneity of M_R among individual BC-containing at each M_p. The results showed that the SD of Case 1 (0.63 ± 0.004) was greater than that of Case 3 (SD = 0.52 ± 0.012), followed by Case 2 (SD = 0.48 ± 0.005). In contrast, the $E_{abs\_measured}$ exhibited an opposite trend, suggesting that greater M_R heterogeneity of BC-containing particles leads to a lower $E_{abs\_measured}$. As shown in Fig. 2d, the discrepancy between the modeled (uniform core-shell Mie model) and the measured E_{abs} increases with SD, with this trend being most pronounced in Case 1, where M_R heterogeneity is highest. This suggests that greater M_R heterogeneity may lead to larger deviations from the uniform core-shell assumption, thereby increasing the mismatch between the modeled and measured E_{abs}. Such discrepancies likely due to the uniform core-shell model's simplified treatment of M_R heterogeneity in BC (Romshoo et al., 2024; Wang et al., 2021c).
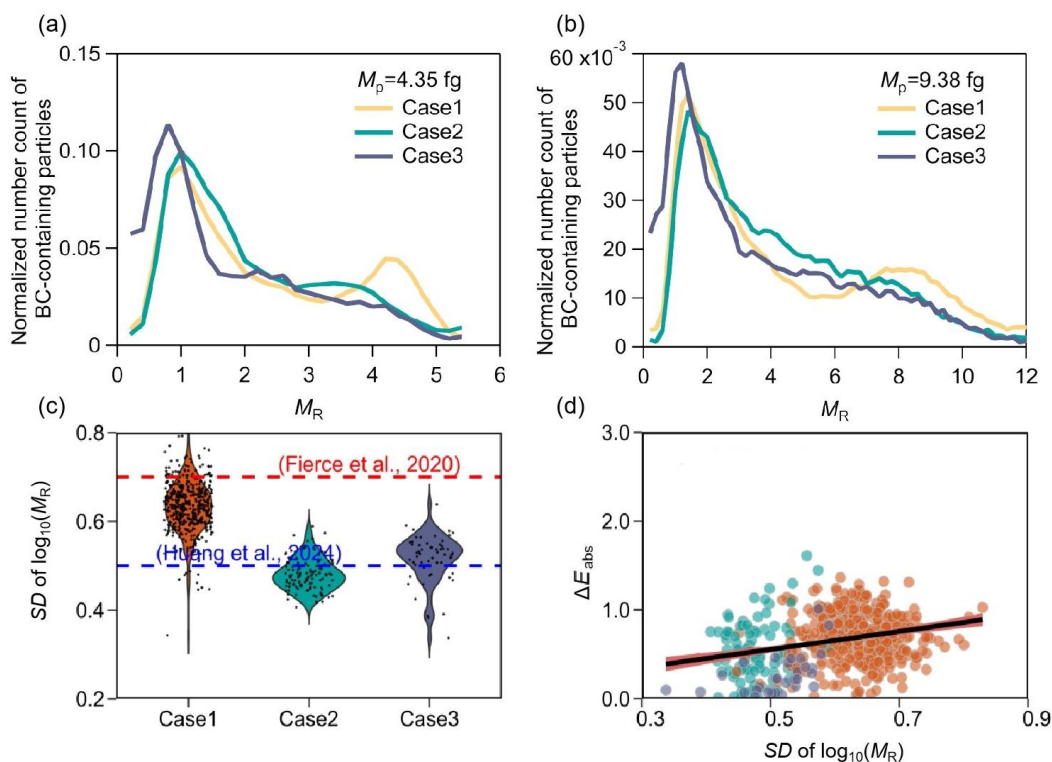
**Figure. 2** M_R heterogeneity of BC-containing particles in different observation periods. The average M_R normalized number distribution of BC-containing particles at $M_p =$ 4.35 fg (**a**) and $M_p = 9.38$ fg (**b**) during different cases. (**c**) Comparison of the average standard deviation (*SD*) of $\log_{10}(M_R)$ in this study with those reported by Huang et al. (2024) and Fierce et al. (2020), the *SD* characterizes the dispersion of M_R among individual BC-containing particles. (**d**) Linear fitting of ΔE_{abs} ($E_{abs\_uniform}$-$E_{abs\_measured}$) with the *SD* of $\log_{10}(M_R)$.

The SP2 measures the scattering cross-section (C_{sca}) of single BC-containing particles. The comparison between measured and the modeled (by Core-shell Mie model) C_{sca} serves as an optical proxy of changes in BC compaction and coating state, reflecting the evolution of optical properties during aging process. Fig. 3 presents the variation of the ratio $C_{sca\_measured}/C_{sca\_modeled}$ at wavelength of 1064 nm with M_R under different M_p. When M_R is relatively low, $C_{sca\_measured}/C_{sca\_modeled}$ is less than 1, suggesting that the BC cores may exist in a fractal structure, remain bare, or are not fully embedded in the coating materials. Consequently, the measured C_{sca} is lower than the C_{sca} predicted by the core-shell Mie model. This observation aligns with Liu et al. (2017a), who classified such BC-containing particles as externally mixed. As M_R increases, $C_{sca\_measured}/C_{sca\_modeled}$ also increases, indicating the BC particles becomes more compact and more thoroughly coated, transitioning toward a core-shell structure (Corbin et al., 2023). Following previous studies (Liu et al., 2017a; Liu et al., 2020), we describe this stage as a "transition state". In this work, the transition state is neither defined by a fixed M_R threshold nor by any directly observed morphological boundary. Instead, it reflects an optically inferred state in which scattering enhancement increases markedly, with M_R ranges of 1.78-6.34 (Case 1), 1.43-3.78 (Case 2), and 1.45-4.19

(Case 3). The higher M_R thresholds observed in Case 2 and Case 3 indicate that under polluted conditions, BC particles can reach an optically core-shell-like state with comparatively less coating material. This likely reflected accelerated aging driven by enhanced secondary formation and condensation of inorganics and organics on BC, facilitated by stagnant meteorological conditions (low wind speed). Such conditions promote efficient coating growth on BC-containing particles, strengthening their light-absorption capability and leading to high E_{abs}. Therefore, compared with Case 1, BC in Case 2 and Case 3 required less coating material to reach the core-shell configuration. When M_R exceeds the transition state range, the ratio $C_{sca\_measured}/C_{sca\_modeled}$ becomes relatively stable, suggesting that the BC particles behave optically like compact, spherical core-shell structures.
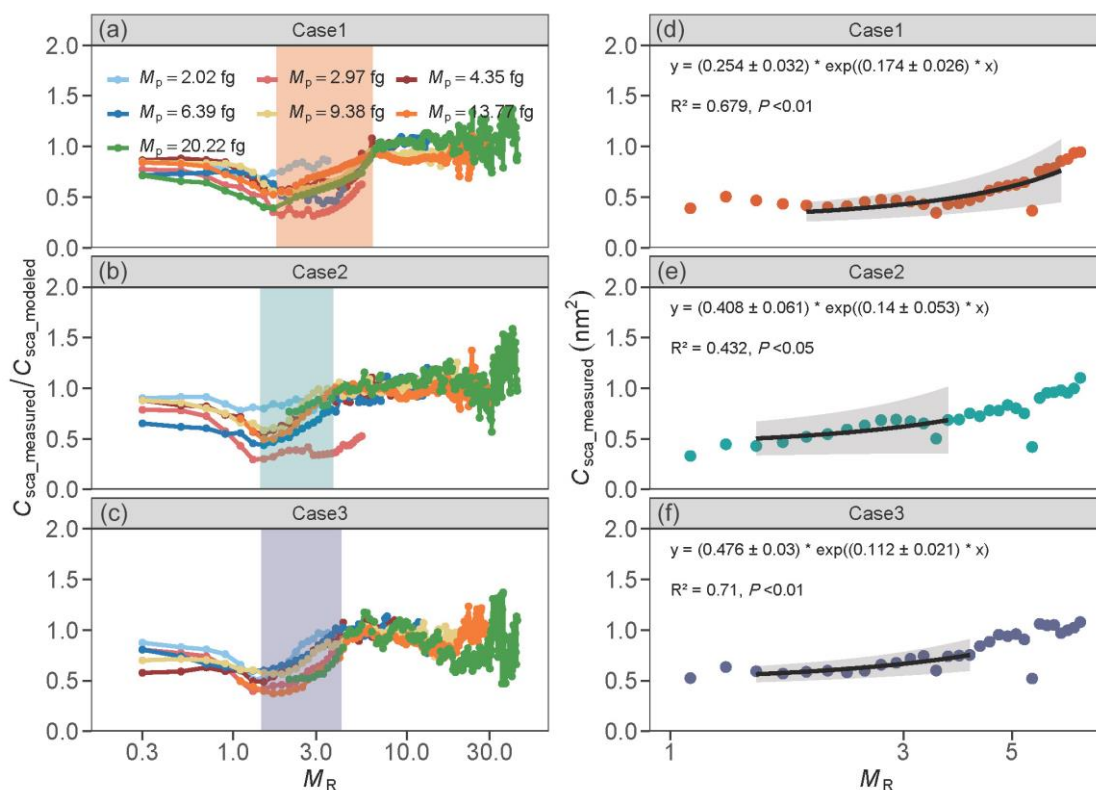
Figure. 3 The optical behavior of BC-containing particles as a function of mass ratio (coating-to-BC, M_R). (**a**) – (**c**) show the ratio of measured to modeled scattering cross-section at the wavelength of 1064 nm during different cases. The shadows indicate the M_R ranges corresponding to "transition-state" BC-containing particles. (**d**) – (**f**) present the measured scattering cross-section as a function of M_R, along with fitted optical transition-dependent models representing the "transition-state" BC-containing particles. The fitted curves include the corresponding P-values, and the shaded areas denote the 95% confidence intervals.

3.3 The predicted E_{abs} during different period.

The complexity of BC in the atmosphere depends on various factors, including the size, the coating amount, and the interaction between the BC core and its coating. In this study, comprehensive multidimensional information on single BC-containing

particle is retrieved and subsequently incorporated into the optical model, as shown in Fig. 4. The bias between $E_{abs\_uniform}$ and $E_{abs\_measured}$ varies across different periods, even when applying the same model input scheme. Specially, the $E_{abs\_uniform}$ agrees with $E_{abs\_measured}$ during Case 2 and Case 3, with deviations below 10%, whereas the deviation increases to as much as to 65% during Case 1, primarily due to the higher M_R dispersion of BC-containing particles in this period. To further investigate this discrepancy, we assume that all BC-containing particles adopt a core-shell structure and calculate the E_{abs} of each BC-containing particle based on the measured single-particle M_R. Subsequently, the E_{abs} of bulk BC-containing particles ($E_{abs\_resolved}$) was determined and compared with $E_{abs\_measured}$ to evaluate their consistency. The results show that for Case 1, although the discrepancy between the measured and modeled values exhibits a decreasing trend, the average deviation remains as high as 38%. This larger deviation, compared to previous particle-resolved modeling studies, is primarily attributed to the smaller dispersion of particle-to-particle M_R observed in Case 1 (Fig. 2c) relative to their model simulations (Fierce et al., 2020). However, for Case 2 and Case 3 with higher M_R heterogeneity of BC-containing particles, the error between the model and measured E_{abs} is almost negligible, with deviations below 10%, indicating that the core-shell Mie model can reproduce the observed E_{abs} during these periods. These findings further validate that the degree of M_R dispersion of BC-containing particles is a key factor in determining whether the core-shell Mie model overestimates the observed E_{abs}, and to what extent this overestimation occurs.
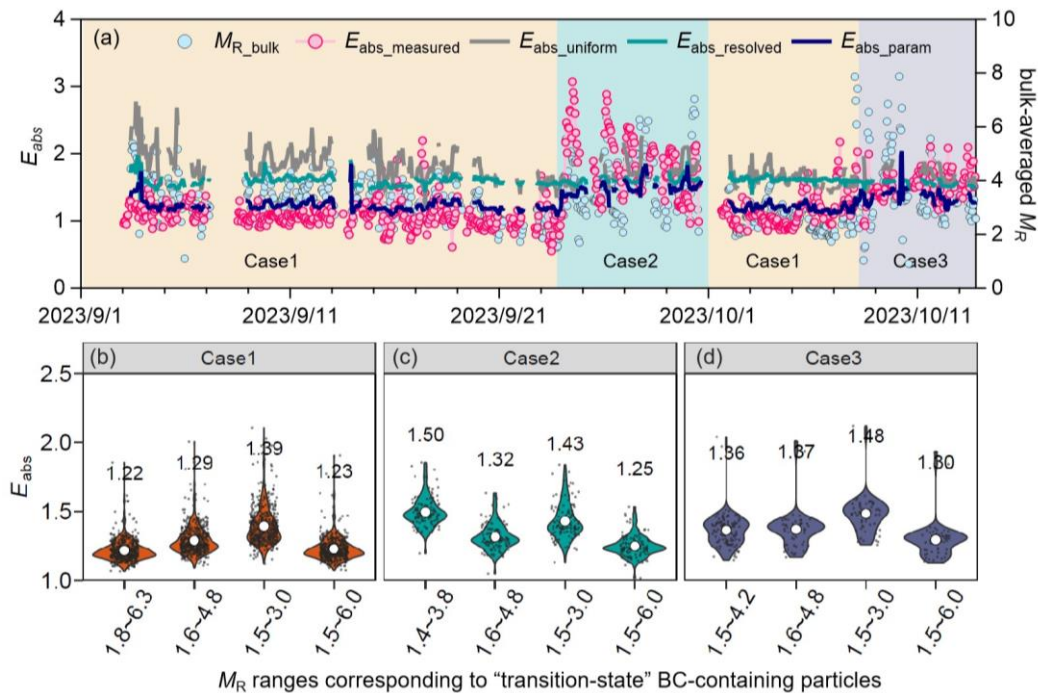
Figure. 4 Comparison of measured and modeled E_{abs} under various different model input schemes. (**a**) shows the time series of the E_{abs} during the observation period. (**b**) – (**d**) were the sensitivity of E_{abs} to the "transition state" range of BC-containing particles. The "transition state" range of 1.6~4.8 was the average value derived from Case 1, Case 2 and Case 3. The range of 1.5~3.0 and 1.5~6.0 was reported by Liu et al. (2017a), and Liu et al. (2020), respectively.

The transitional-state particles are BC-containing particles in the process of evolving from loosely aggregated fractal-like structures toward quasi–core–shell configurations (Moffet et al., 2016; Moteki and Kondo, 2007). The abundance of transitional-state particles varies notably under different atmospheric conditions, directly influencing the measured E_{abs} (Liu et al., 2017a). During clean days (Case 1), the atmospheric environment was characterized by low PM_1 concentrations, weak secondary formation, and highly variable coating conditions. Under such conditions, our measurements show that BC-containing particles were dominated by transitional-state structures (Fig. S9), representing the intermediate stage between externally mixed aggregates and fully developed quasi–core–shell structures. The limited and heterogeneous coating distribution on these particles substantially weakens the lensing effect, resulting in lower measured E_{abs} (Peng et al., 2016). Because the core-shell Mie model inherently assumes a uniform and concentric coating, it does not accurately represent the optical behavior of these transitional particles, leading to a pronounced overestimation of measured E_{abs} during Case 1. This indicates that, under clean conditions, the optical properties of transitional-state particles are the key driver of the model-observation discrepancy. In contrast, the haze period (Case 2) represents a more aged and heavily coated aerosol environment and provides a useful reference for understanding the factors influencing the measured E_{abs}. During Case 2, the high aerosol loading and elevated bulk-averaged M_R were largely influenced by regional transport, as air masses at 100 m, 500 m, and 1000 m all followed similar pathways from the northern Yangtze River Delta into northern Zhejiang (Fig. 1c and Fig. S7). Stagnant meteorological conditions, elevated relative humidity, and enhanced oxidative capacity further facilitated vigorous liquid-phase and photochemical reactions, promoting the abundant formation of secondary coatings on BC surfaces (Peng et al., 2016). Notably, our observations show that E_{abs} increases systematically with the increasing contribution of secondary nitrate (Fig. S8), consistent with the fact that nitrate-rich conditions enhance aqueous-phase oxidation and accelerate the formation of thick inorganic coatings (Liu et al., 2017b). As a result, a much larger fraction of BC-containing particles exhibited internally mixed, quasi–core-shell structures rather than transitional states (Fig. S9), which explains why the core-shell Mie model performs substantially better for Case 2 than for Case 1. This contrast reinforces the central role of transitional-state particles in determining measured E_{abs} when coatings are sparse, irregular, or partially developed. Given the strong influence of transitional-state particles on measured E_{abs} in Case 1, precise constraints on their optical behavior are crucial for improving E_{abs} estimates across different atmospheric scenarios. To address this, an empirical formula based on optical measurements was developed to estimate the E_{abs} of BC-containing particles in the "transition state", derived from fitting the measured C_{sca} against M_R (Fig. 3d-3f). By applying this empirical formula to the calculation of E_{abs}, the resulting value for Case 1 was 1.21 ± 0.01. For Case 2 and Case 3, the E_{abs} calculated using the same formula (E_{abs_param}) remained slightly lower than the $E_{abs\_measured}$, but the deviation was within 20%, demonstrating the reliability of the approach across different atmospheric conditions.

In recent years, particle-resolved models have been increasingly applied in field

observations to mitigate the well-known overestimation of E_{abs} by uniform core-shell Mie model (Fierce et al., 2020; Li et al., 2024; Jiang et al., 2025). Some studies have incorporated particle-specific structural detail using approaches such as the electron-microscope-to-BC-simulation (EMBS) framework (Wang et al., 2021c; Wang et al., 2021b; Chakrabarty et al., 2006), which further improves the representation of BC absorption. In this study, we introduce an observationally constrained parameterization that links SP2-measured scattering cross sections with core-shell Mie calculations. This scheme identifies the optical transition state through following steps: (1) measuring single-particle C_{sca} with SP2, (2) fitting the relationship between $C_{sca\_measured}$ and M_R (Fig. 4b-4c), (3) identifying the M_R range associated with transitional optical behavior ("transition state"), and (4) inferring the MAC of transition-state particles using the fitted relationship before integrating MAC over all particles to obtain bulk E_{abs}. This parameterization improves agreement with observations, especially during clean periods (Case 1), when the uniform core-shell assumption tends to produce the largest discrepancies. However, its performance depends on correctly identifying the M_R range of the transition state. Our results show that, in polluted periods (Cases 2 and 3), the M_R range associated with the transition-state becomes relatively narrow, while under clean conditions it tends to expand. Consequently, applying a fixed M_R threshold across all atmospheric conditions can introduce systematic biases in modeled E_{abs} (Fig. 4b, c and d). Although M_R heterogeneity alone can adequately reproduce E_{abs} during polluted periods, adopting separate input schemes for different environments would complicate radiative transfer calculations and limit broader applicability.

To address this issue, we emphasize that the proposed framework is adaptable to environments in which BC particles undergo similar optical transitions. Key parameters, including the M_R thresholds that define the transition state and other indicators derived from the $C_{sca\_measured}$-M_R relationship, can be recalibrated for different atmospheric contexts. This includes rural aeras, biomass-burning regions, or seasons with distinct pollution characteristics, where coating composition and aging processes may vary. Although the parameterization is fundamentally based on the optical evolution of BC from loosely coated to more compact states, it can be adjusted to account for local differences in particle coating and aging dynamics. Thus, the unified scheme incorporates both M_R variability and optical characteristics of transitional particles, providing a flexible and physically consistent approach for a wide range of atmospheric environments. Overall, this observationally constrained approach offers a more consistent representation of BC mixing states across diverse atmospheric conditions, thereby reducing uncertainties in optical modeling and enhancing the reliability of BC radiative effect assessments.

4 Conclusions

In this study, we employed the CPMA-SP2 tandem system to investigate the mass ratio of coating to core (M_R) of BC-containing particles in Hangzhou, China, and to assess how M_R heterogeneity and optical transitions influence their E_{abs} under different atmospheric conditions. By dividing the observation into three representative scenarios (Case 1, Case 2, and Case 3), we identified significant differences in the measured E_{abs}

that are closely associated with the evolution and distribution of M_R. The results indicate that both M_R heterogeneity and optical effects of BC-containing particles in the transition state are critical for accurately modeling BC E_{abs}. During clean periods (Case 1), the uniform core-shell Mie model significantly overestimated E_{abs}, while during polluted periods (Case 2 and Case 3), model predictions were more consistent with the measured E_{abs}. To address these discrepancies, we developed an observationally constrained parameterization for BC particles in the transition state based on the transitional optical behavior. This scheme effectively reconciles modeled and measured E_{abs} across different pollution scenarios, particularly in clean periods dominated by externally mixed or partially coated BC-containing particles. These results highlight the limitations of uniform model input schemes under complex atmospheric conditions and underscore the value of a unified parameterization framework that accounts for both M_R heterogeneity and the optical properties of transition-state particles. By incorporating M_R-dependent optical transitions, this framework provides an adaptable approach for representing BC mixing states and light absorption under different atmospheric environments. This parameterization improves the consistency between modeled and observed E_{abs} and reduces uncertainties in assessing the radiative effects of BC-containing particles, offering a flexible tool for application to other atmospheric conditions.

Data availability. The data are available from the link: http://doi.org/10.6084/m9.figshare.29097263.

Author contributions.

Conceptualization: Jing Wei, Zhi-Bin Wang
Data curation: Jing Wei, Yao Song, Xiang-Yu Pei, Fei Zhang, Zheng-Ning Xu, Jin-Mei Ding, Xiao-Yuan Wang, Sheng-Chen Xu, Xu-Dong Tian, Bing-Ye Xu
Formal analysis: Jing Wei
Funding acquisition: Zhi-Bin Wang, Bing-Ye Xu
Investigation: Zhi-Bin Wang
Methodology: Jing Wei, Zhi-Bin Wang
Visualization: Jing Wei, Zhi-Bin Wang
Writing – original draft: Jing Wei

Competing interests. At least one of the (co-)authors is a member of the editorial board of *Atmospheric Chemistry and Physics*.

References

Adachi, K. and Buseck, P. R.: Changes of ns-soot mixing states and shapes in an urban area during CalNex, Journal of Geophysical Research-Atmospheres, 118, 3723-3730, 10.1002/jgrd.50321, 2013.

Adachi, K., Chung, S. H., and Buseck, P. R.: Shapes of soot aerosol particles and implications for their effects on climate, Journal of Geophysical Research: Atmospheres, 115, D15206, 10.1029/2009jd012868, 2010.

Adachi, K., Moteki, N., Kondo, Y., and Igarashi, Y.: Mixing states of light-absorbing particles measured using a transmission electron microscope and a single-particle soot photometer in Tokyo, Japan, Journal of Geophysical Research-Atmospheres, 121, 9153-9164, 10.1002/2016jd025153, 2016.

Bauer, S. E., Ault, A. P., and Prather, K. A.: Evaluation of aerosol mixing state classes in the GISS modelE-MATRIX climate model using single-particle mass spectrometry measurements, Journal of Geophysical Research: Atmospheres, 118, 9834-9844, 10.1002/jgrd.50700, 2013.

Baumgardner, D., Popovicheva, O., Allan, J., Bernardoni, V., Cao, J., Cavalli, F., Cozic, J., Diapouli, E., Eleftheriadis, K., Genberg, P. J., Gonzalez, C., Gysel, M., John, A., Kirchstetter, T. W., Kuhlbusch, T. A. J., Laborde, M., Lack, D., Müller, T., Niessner, R., Petzold, A., Piazzalunga, A., Putaud, J. P., Schwarz, J., Sheridan, P., Subramanian, R., Swietlicki, E., Valli, G., Vecchi, R., and Viana, M.: Soot reference materials for instrument calibration and intercomparisons: a workshop summary with recommendations, Atmospheric Measurement Techniques, 5, 1869-1887, 10.5194/amt-5-1869-2012, 2012.

Beeler, P., Kumar, J., Schwarz, J. P., Adachi, K., Fierce, L., Perring, A. E., Katich, J. M., and Chakrabarty, R. K.: Light absorption enhancement of black carbon in a pyrocumulonimbus cloud, Nature Communications, 15, 10.1038/s41467-024-50070-0, 2024.

Bond, T. C. and Bergstrom, R. W.: Light Absorption by Carbonaceous Particles: An Investigative Review, Aerosol Science and Technology, 40, 27-67, 10.1080/02786820500421521, 2006.

Brooks, J., Liu, D., Allan, J. D., Williams, P. I., Haywood, J., Highwood, E. J., Kompalli, S. K., Babu, S. S., Satheesh, S. K., Turner, A. G., and Coe, H.: Black carbon physical and optical properties across northern India during pre-monsoon and monsoon seasons, Atmospheric Chemistry and Physics, 19, 13079-13096, 10.5194/acp-19-13079-2019., 2019.

Cappa, C. D., Zhang, X., Russell, L. M., Collier, S., Lee, A. K. Y., Chen, C. L., Betha, R., Chen, S., Liu, J., Price, D. J., Sanchez, K. J., McMeeking, G. R., Williams, L. R., Onasch, T. B., Worsnop, D. R., Abbatt, J., and Zhang, Q.: Light Absorption by Ambient Black and Brown Carbon and its Dependence on Black Carbon Coating State for Two California, USA, Cities in Winter and Summer, Journal of Geophysical Research: Atmospheres, 124, 1550-1577, 10.1029/2018JD029501, 2019.

Cappa, C. D., Onasch, T. B., Massoli, P., Worsnop, D. R., Bates, T. S., Cross, E. S., Davidovits, P., Hakala, J., Hayden, K. L., Jobson, B. T., Kolesar, K. R., Lack, D. A., Lerner, B. M., Li, S.-M., Mellon, D., Nuaaman, I., Olfert, J. S., Petäjä, T., Quinn, P. K., Song, C., Subramanian, R., Williams, E. J., and Zaveri, R. A.: Radiative Absorption Enhancements Due to the Mixing State of Atmospheric Black Carbon, Science, 337, 1078-1081, https://doi.org/10.1126/science.1223447, 2012.

Chakrabarty, R. K., Moosmueller, H., Arnott, W. P., Garro, M. A., and Walker, J.: Structural and fractal properties of particles emitted from spark ignition engines, Environmental Science & Technology, 40, 6647-6654, 10.1021/es060537y, 2006.

Chen, G., Liu, C., Wang, J., Yin, Y., and Wang, Y.: Accounting for Black Carbon Mixing State,

Nonsphericity, and Heterogeneity Effects in Its Optical Property Parameterization in a Climate Model, Journal of Geophysical Research: Atmospheres, 129, e2024JD041135, 10.1029/2024JD041135, 2024.

China, S., Mazzoleni, C., Gorkowski, K., Aiken, A. C., Dubey, M. K., and Michigan Technological Univ, H. M. I.: Morphology and mixing state of individual freshly emitted wildfire carbonaceous particles, Nature Communications, 4, 2122-2122, 10.1038/ncomms3122, 2013.

Corbin, J. C., Modini, R. L., and Gysel-Beer, M.: Mechanisms of soot-aggregate restructuring and compaction, Aerosol Science and Technology, 57, 89-111, 10.1080/02786826.2022.2137385, 2023.

Cross, E. S., Onasch, T. B., Ahern, A., Wrobel, W., Slowik, J. G., Olfert, J., Lack, D. A., Massoli, P., Cappa, C. D., Schwarz, J. P., Spackman, J. R., Fahey, D. W., Sedlacek, A., Trimborn, A., Jayne, J. T., Freedman, A., Williams, L. R., Ng, N. L., Mazzoleni, C., Dubey, M., Brem, B., Kok, G., Subramanian, R., Freitag, S., Clarke, A., Thornhill, D., Marr, L. C., Kolb, C. E., Worsnop, D. R., and Davidovits, P.: Soot Particle StudiesInstrument Inter-ComparisonProject Overview, Aerosol Science and Technology, 44, 592-611, 10.1080/02786826.2010.482113, 2010.

Fierce, L., Onasch, T. B., Cappa, C. D., Mazzoleni, C., China, S., Bhandari, J., Davidovits, P., Al Fischer, D., Helgestad, T., Lambe, A. T., Sedlacek, A. J., Smith, G. D., Wolff, L., Brookhaven National Lab, U. N. Y., and Pacific Northwest National Lab, R. W. A.: Radiative absorption enhancements by black carbon controlled by particle-to-particle heterogeneity in composition, Proceedings of the National Academy of Sciences, 117, 5196-5203, 10.1073/pnas.1919723117, 2020.

Gao, R. S., Schwarz, J. P., Kelly, K. K., Fahey, D. W., Watts, L. A., Thompson, T. L., Spackman, J. R., Slowik, J. G., Cross, E. S., Han, J. H., Davidovits, P., Onasch, T. B., and Worsnop, D. R.: A Novel Method for Estimating Light-Scattering Properties of Soot Aerosols Using a Modified Single-Particle Soot Photometer, Aerosol Science and Technology, 41, 125-135, 10.1080/02786820601118398, 2007.

Gysel, M., Laborde, M., Olfert, J. S., Subramanian, R., and Gröhn, A. J.: Effective density of Aquadag and fullerene soot black carbon reference materials used for SP2 calibration, Atmospheric Measurement Techniques, 4, 2851-2858, 10.5194/amt-4-2851-2011, 2011.

Huang, X.-F., Peng, Y., Wei, J., Peng, J., Lin, X.-Y., Tang, M.-X., Cheng, Y., Men, Z., Fang, T., Zhang, J., He, L.-Y., Cao, L. M., Liu, C., Zhang, C., Mao, H., Seinfeld, J. H., and Wang, Y.: Microphysical complexity of black carbon particles restricts their warming potential, One Earth, 7, 10.1016/j.oneear.2023.12.004, 2024.

Jiang, F., Zheng, Z., Coe, H., Healy, R. M., Poulain, L., Gros, V., Zhang, H., Li, W., Liu, D., West, M., Topping, D., and Riemer, N.: Integrating Simulations and Observations: A Foundation Model for Estimating the Aerosol Mixing State Index, Environmental Science & Technology Air, 10.1021/acsestair.4c00329, 2025.

Kahnert, M. and Kanngießer, F.: Modelling optical properties of atmospheric black carbon aerosols, Journal of Quantitative Spectroscopy & Radiative Transfer, 244, 106849, 10.1016/j.jqsrt.2020.106849, 2020.

Laborde, M., Schnaiter, M., Linke, C., Saathoff, H., Naumann, K. H., Möhler, O., Berlenz, S., Wagner, U., Taylor, J. W., Liu, D., Flynn, M., Allan, J. D., Coe, H., Heimerl, K., Dahlkötter, F., Weinzierl, B., Wollny, A. G., Zanatta, M., Cozic, J., Laj, P., Hitzenberger, R., Schwarz, J. P., and Gysel, M.: Single Particle Soot Photometer intercomparison at the AIDA chamber, Atmospheric Measurement Techniques, 5, 3077-3097, 10.5194/amt-5-3077-2012, 2012.

Li, W., Riemer, N., Xu, L., Wang, Y., Adachi, K., Shi, Z., Zhang, D., Zheng, Z., and Laskin, A.:

Microphysical properties of atmospheric soot and organic particles: measurements, modeling, and impacts, npj Climate and Atmospheric Science, 7, 65, 10.1038/s41612-024-00610-8, 2024.

Liu, D., Taylor, J. W., Young, D. E., Flynn, M. J., Coe, H., and Allan, J. D.: The effect of complex black carbon microphysics on the determination of the optical properties of brown carbon: BC morphology on BrC optical properties, Geophysical Research Letters, 42, 613-619, 10.1002/2014GL062443, 2015a.

Liu, D., Allan, J. D., Young, D. E., Coe, H., Beddows, D., Fleming, Z. L., Flynn, M. J., Gallagher, M. W., Harrison, R. M., Lee, J., Prevot, A. S. H., Taylor, J. W., Yin, J., Williams, P. I., and Zotter, P.: Size distribution, mixing state and source apportionment of black carbon aerosol in London during wintertime, Atmospheric Chemistry and Physics, 14, 10061-10084, 10.5194/acp-14-10061-2014, 2014.

Liu, D., Whitehead, J., Alfarra, M. R., Reyes-Villegas, E., Spracklen, D. V., Reddington, C. L., Kong, S., Williams, P. I., Ting, Y.-C., Haslett, S., Taylor, J. W., Flynn, M. J., Morgan, W. T., McFiggans, G., Coe, H., and Allan, J. D.: Black-carbon absorption enhancement in the atmosphere determined by particle mixing state, Nature Geoscience, 10, 184-188, 10.1038/ngeo2901, 2017a.

Liu, H., Pan, X., Liu, D., Liu, X., Chen, X., Tian, Y., Sun, Y., Fu, P., and Wang, Z.: Mixing characteristics of refractory black carbon aerosols at an urban site in Beijing, Atmospheric Chemistry and Physics, 20, 5771-5785, 10.5194/acp-20-5771-2020, 2020.

Liu, H., Pan, X. L., Wang, D. W., Liu, X. Y., Tian, Y., Yao, W. J., Lei, S. D., Zhang, Y. T., Li, J., Lei, L., Xie, C. H., Fu, P. Q., Sun, Y. L., and Wang, Z. F.: Mixing characteristics of black carbon aerosols in a coastal city using the CPMA-SP2 system, Atmospheric Research, 265, 10.1016/j.atmosres.2021.105867, 2022.

Liu, S., Aiken, A. C., Gorkowski, K., Dubey, M. K., Cappa, C. D., Williams, L. R., Herndon, S. C., Massoli, P., Fortner, E. C., Chhabra, P. S., Brooks, W. A., Onasch, T. B., Jayne, J. T., Worsnop, D. R., China, S., Sharma, N., Mazzoleni, C., Xu, L., Ng, N. L., Liu, D., Allan, J. D., Lee, J. D., Fleming, Z. L., Mohr, C., Zotter, P., Szidat, S., Prévôt, A. S. H., Los Alamos National Lab, L. A. N. M., and Univ. of California, D. C. A.: Enhanced light absorption by mixed source black and brown carbon particles in UK winter, Nature Communications, 6, 8435-8435, 10.1038/ncomms9435, 2015b.

Liu, Y., Wu, Z., Wang, Y., Xiao, Y., Gu, F., Zheng, J., Tan, T., Shang, D., Wu, Y., Zeng, L., Hu, M., Bateman, A. P., and Martin, S. T.: Submicrometer Particles Are in the Liquid State during Heavy Haze Episodes in the Urban Atmosphere of Beijing, China, Environmental Science & Technology Letters, 4, 427-432, 10.1021/acs.estlett.7b00352, 2017b.

Modini, R. L., Corbin, J. C., Brem, B. T., Irwin, M., Bertò, M., Pileci, R. E., Fetfatzis, P., Eleftheriadis, K., Henzing, B., Moerman, M. M., Liu, F., Müller, T., and Gysel-Beer, M.: Detailed characterization of the CAPS single-scattering albedo monitor (CAPS PMssa) as a field-deployable instrument for measuring aerosol light absorption with the extinction-minus-scattering method, Atmos. Meas. Tech., 14, 819-851, 10.5194/amt-14-819-2021, 2021.

Moffet, R. C., O'Brien, R. E., Alpert, P. A., Kelly, S. T., Pham, D. Q., Gilles, M. K., Knopf, D. A., Laskin, A., Pacific Northwest National Lab, R. W. A. E. M. S. L., Lawrence Berkeley National Lab, B. C. A., and Stony Brook Univ, S. B. N. Y.: Morphology and mixing of black carbon particles collected in central California during the CARES field study, Atmospheric chemistry and physics, 16, 14515-14525, 10.5194/acp-16-14515-2016, 2016.

Moteki, N. and Kondo, Y.: Effects of Mixing State on Black Carbon Measurements by Laser-Induced Incandescence, Aerosol Science and Technology, 41, 398-417, 10.1080/02786820701199728, 2007.

Moteki, N. and Kondo, Y.: Dependence of Laser-Induced Incandescence on Physical Properties of Black Carbon Aerosols: Measurements and Theoretical Interpretation, Aerosol Science and Technology, 44, 663-675, 10.1080/02786826.2010.484450, 2010.

Naseri, A., Corbin, J. C., and Olfert, J. S.: Comparison of the LEO and CPMA-SP2 techniques for black-carbon mixing-state measurements, Atmos. Meas. Tech., 17, 3719-3738, 10.5194/amt-17-3719-2024, 2024.

Naseri, A., Sipkens, T. A., Rogak, S. N., and Olfert, J. S.: An improved inversion method for determining two-dimensional mass distributions of non-refractory materials on refractory black carbon, Aerosol Science and Technology, 55, 104-118, 10.1080/02786826.2020.1825615, 2021.

Naseri, A., Sipkens, T. A., Rogak, S. N., and Olfert, J. S.: Optimized instrument configurations for tandem particle mass analyzer and single particle-soot photometer experiments, Journal of Aerosol Science, 160, 10.1016/j.jaerosci.2021.105897, 2022.

Olfert, J. S. and Collings, N.: New method for particle mass classification - the Couette centrifugal particle mass analyzer, Journal of Aerosol Science, 36, 1338-1352, 10.1016/j.jaerosci.2005.03.006, 2005.

Peng, J., Hu, M., Guo, S., Du, Z., Zheng, J., Shang, D., Zamora, M. L., Zeng, L., Shao, M., Wu, Y.-S., Zheng, J., Wang, Y., Glen, C. R., Collins, D. R., Molina, M. J., and Zhang, R.: Markedly enhanced absorption and direct radiative forcing of black carbon under polluted urban environments, Proceedings of the National Academy of Sciences, 113, 4266-4271, 10.1073/pnas.1602310113, 2016.

Qian, H., Xu, B., Xu, Z., Zou, Q., Zi, Q., Zuo, H., Zhang, F., Wei, J., Pei, X., Zhou, W., Jin, L., Tian, X., Zhao, W., and Wang, Z.: Anthropogenic Oxygenated Volatile Organic Compounds Dominate Atmospheric Oxidation Capacity and Ozone Production via Secondary Formation of Formaldehyde in the Urban Atmosphere, ACS ES&T Air, 2, 1033-1041, 10.1021/acsestair.4c00317, 2025.

Radney, J. G., You, R. A., Ma, X. F., Conny, J. M., Zachariah, M. R., Hodges, J. T., and Zangmeister, C. D.: Dependence of Soot Optical Properties on Particle Morphology: Measurements and Model Comparisons, Environmental Science & Technology, 48, 3169-3176, 10.1021/es4041804, 2014.

Romshoo, B., Müller, T., Ahlawat, A., Wiedensohler, A., Haneef, M. V., Imran, M., Warsi, A. B., Mandariya, A. K., Habib, G., and Pöhlker, M. L.: Significant contribution of fractal morphology to aerosol light absorption in polluted environments dominated by black carbon (BC), npj Climate and Atmospheric Science, 7, 87, 10.1038/s41612-024-00634-0, 2024.

Schloesser, H.: Use of a Multi-Wavelength Integrating Nephelometer to Determine Source Influences on Particle Concentration Measurements. Atmospheric optics: aerosols, visibility and the radiativ balance 2016, vol. 1: Atmospheric optics conference, 27-30 September 2016, Jackson Hole, Wyoming, USA., 2016.

Schwarz, J. P., Katich, J. M., Lee, S. L., Thomson, D. S., and Watts, L. A.: "Invisible bias" in the single particle soot photometer due to trigger deadtime, Aerosol Science and Technology, 56, 623-635, 10.1080/02786826.2022.2064265, 2022.

Seinfeld, J.: Atmospheric science - Black carbon and brown clouds, Nature Geoscience, 1, 15-16, 10.1038/ngeo.2007.62, 2008.

Stephens, M., Turner, N., and Sandberg, J.: Particle identification by laser-induced incandescence in a solid-state laser cavity, Applied Optics, 42, 3726-3736, 10.1364/ao.42.003726, 2003.

Stier, P., Feichter, J., Kinne, S., Kloster, S., Vignati, E., Wilson, J., Ganzeveld, L., Tegen, I., Werner, M., Balkanski, Y., Schulz, M., Boucher, O., Minikin, A., and Petzold, A.: The aerosol-climate model

ECHAM5-HAM, Atmospheric Chemistry and Physics, 5, 1125-1156, 10.5194/acp-5-1125-2005, 2005.

Szopa, S., Naik, V., Adhikary, B., Artaxo, P., Berntsen, T., Collins, W. D., Fuzzi, S., Gallardo, L., Kiendler-Scharr, A., Klimont, Z., Liao, H., Unger, N., and Zanis, P.: Short-Lived Climate Forcers. In Climate Change 2021: The Physical Science Basis. Contribution of Working Group I to the Sixth Assessment Report of the Intergovernmental Panel on Climate Change (eds Masson-Delmotte, V. et al.), IPCC, 2021.

Ueda, S., Nakayama, T., Taketani, F., Adachi, K., Matsuki, A., Iwamoto, Y., Sadanaga, Y., and Matsumi, Y.: Light absorption and morphological properties of soot-containing aerosols observed at an East Asian outflow site, Noto Peninsula, Japan, Atmospheric chemistry and physics, 16, 2525-2541, 10.5194/acp-16-2525-2016, 2016.

Wang, J., Wang, J., Cai, R., Liu, C., Jiang, J., Nie, W., Wang, J., Moteki, N., Zaveri, R. A., Huang, X., Ma, N., Chen, G., Wang, Z., Jin, Y., Cai, J., Zhang, Y., Chi, X., Holanda, B. A., Xing, J., Liu, T., Qi, X., Wang, Q., Pöhlker, C., Su, H., Cheng, Y., Wang, S., Hao, J., Andreae, M. O., and Ding, A.: Unified theoretical framework for black carbon mixing state allows greater accuracy of climate effect estimation, Nature Communications, 14, 2703, 10.1038/s41467-023-38330-x, 2023.

Wang, T. T., Zhao, G., Tan, T. Y., Yu, Y., Tang, R. Z., Dong, H. B., Chen, S. Y., Li, X., Lu, K. D., Zeng, L. M., Gao, Y. Q., Wang, H. L., Lou, S. R., Liu, D. T., Hu, M., Zhao, C. S., and Guo, S.: Effects of biomass burning and photochemical oxidation on the black carbon mixing state and light absorption in summer season, Atmospheric Environment, 248, 10.1016/j.atmosenv.2021.118230, 2021a.

Wang, Y., Pang, Y., Huang, J., Bi, L., Che, H., Zhang, X., and Li, W.: Constructing Shapes and Mixing Structures of Black Carbon Particles With Applications to Optical Calculations, Journal of Geophysical Research: Atmospheres, 126, 10.1029/2021jd034620, 2021b.

Wang, Y., Li, W., Huang, J., Liu, L., Pang, Y., He, C., Liu, F., Liu, D., Bi, L., Zhang, X., and Shi, Z.: Nonlinear Enhancement of Radiative Absorption by Black Carbon in Response to Particle Mixing Structure, Geophysical Research Letters, 48, 10.1029/2021gl096437, 2021c.

Weber, P., Petzold, A., Bischof, O. F., Fischer, B., Berg, M., Freedman, A., Onasch, T. B., and Bundke, U.: Relative errors in derived multi-wavelength intensive aerosol optical properties using cavity attenuated phase shift single-scattering albedo monitors, a nephelometer, and tricolour absorption photometer measurements, Atmospheric Measurement Techniques, 15, 3279-3296, 10.5194/amt-15-3279-2022, 2022.

Wu, Y., Cheng, T., and Zheng, L.: Light absorption of black carbon aerosols strongly influenced by particle morphology distribution, Environmental Research Letters, 15, 94051, 10.1088/1748-9326/aba2ff, 2020.

Zanatta, M., Gysel, N., Bukowiecki, T., Müller, E., and Weingartner: A European aerosol phenomenology-5: Climatology of black carbon optical properties at 9 regional background sites across Europe, Atmospheric Environment, 2016.

Zanatta, M., Bogert, P., Ginot, P., Gong, Y., Hoshyaripour, G. A., Hu, Y., Jiang, F., Laj, P., Li, Y., Linke, C., Möhler, O., Saathoff, H., Schnaiter, M., Umo, N. S., Vogel, F., and Wagner, R.: AIDA Arctic transport experiment – Part 1: Simulation of northward transport and aging effect on fundamental black carbon properties, Aerosol Research, 3, 477-502, 10.5194/ar-3-477-2025, 2025.

Zeng, L., Tan, T., Zhao, G., Du, Z., Hu, S., Shang, D., and Hu, M.: Overestimation of black carbon light absorption due to mixing state heterogeneity, npj Climate and Atmospheric Science, 7, 2, 10.1038/s41612-023-00535-8, 2024.

21

Zhai, J., Yang, X., Li, L., Bai, B., Liu, P., Huang, Y., Fu, T.-M., Zhu, L., Zeng, Z., Tao, S., Lu, X., Ye, X., Wang, X., Wang, L., and Chen, J.: Absorption Enhancement of Black Carbon Aerosols Constrained by Mixing-State Heterogeneity, Environmental Science & Technology, 56, 1586-1593, 10.1021/acs.est.1c06180, 2022.

Zhang, F., Shen, J., Xu, D., Shen, J., Qin, Y., Shi, R., Wei, J., Xu, Z., Pei, X., Tang, Q., Chen, H., Xu, B., and Wang, Z.: Unveiling the key drivers and formation pathways for secondary organic aerosols in an eastern China megacity, Journal of Hazardous Materials, 498, 10.1016/j.jhazmat.2025.139925, 2025a.

Zhang, J., Wang, Y., Teng, X., Liu, L., Xu, Y., Ren, L., Shi, Z., Zhang, Y., Jiang, J., Liu, D., Hu, M., Shao, L., Chen, J., Martin, S. T., Zhang, X., and Li, W.: Liquid-liquid phase separation reduces radiative absorption by aged black carbon aerosols, Communications Earth & Environment, 3, 128, 10.1038/s43247-022-00462-1, 2022.

Zhang, R. Y., Khalizov, A. F., Pagels, J., Zhang, D., Xue, H. X., and McMurry, P. H.: Variability in morphology, hygroscopicity, and optical properties of soot aerosols during atmospheric processing, Proc. Natl. Acad. Sci. U. S. A., 105, 10291-10296, 10.1073/pnas.0804860105, 2008.

Zhang, Y., Zhang, Q., Cheng, Y., Su, H., Li, H., Li, M., Zhang, X., Ding, A., and He, K.: Amplification of light absorption of black carbon associated with air pollution, Atmospheric Chemistry and Physics, 18, 9879-9896, 10.5194/acp-18-9879-2018, 2018.

Zhang, Y., Zhang, Q., Cheng, Y., Su, H., Kecorius, S., Wang, Z., Wu, Z., Hu, M., Zhu, T., Wiedensohler, A., and He, K.: Measuring the morphology and density of internally mixed black carbon with SP2 and VTDMA: new insight into the absorption enhancement of black carbon in the atmosphere, Atmospheric Measurement Techniques, 9, 1833-1843, 10.5194/amt-9-1833-2016, 2016.

Zhang, Y. X., Zhang, Q., Yao, Z. L., and Li, H. Y.: Particle Size and Mixing State of Freshly Emitted Black Carbon from Different Combustion Sources in China, Environmental Science & Technology, 54, 7766-7774, 10.1021/acs.est.9b07373, 2020.

Zhang, Z., Wang, J., Wang, J., Riemer, N., Liu, C., Jin, Y., Tian, Z., Cai, J., Cheng, Y., Chen, G., Wang, B., Wang, S., and Ding, A.: Steady-state mixing state of black carbon aerosols from a particle-resolved model, Atmospheric Chemistry and Physics, 25, 1869-1881, 10.5194/acp-25-1869-2025, 2025b.

Zhao, G., Shen, C., and Zhao, C.: Technical note: Mismeasurement of the core-shell structure of black carbon-containing ambient aerosols by SP2 measurements, Atmospheric Environment, 243, 117885, 10.1016/j.atmosenv.2020.117885, 2020.